The formal publication can be found here:
http://dx.doi.org/10.1016/j.commatsci.2015.12.014

Structure and properties of liquid Al-Cu alloys: empirical potentials compared

Jacek Dziedzic[a,b], Szymon Winczewski[a], Jarosław Rybicki[a,c]

[a] *Faculty of Applied Physics and Mathematics, Gdansk University of Technology, Narutowicza 11/12, 80-952 Gdańsk, Poland.*
[b] *School of Chemistry, University of Southampton, Highfield, Southampton SO17 1BJ, UK*
[c] *TASK Computer Centre, Gdansk University of Technology, Narutowicza 11/12, 80-952 Gdańsk, Poland*

Abstract

We report on the structure and mass transport properties of liquid Al-Cu alloys predicted by two recently-developed empirical many-body potentials: MEAM [Jelinek *et al.*, Phys. Rev. B **85** 245102 (2012)] and EAM-ADP [Apostol *et al.*, Phys. Rev. B **83** 054116 (2011)], and by the well-known Gupta potential. Total and partial pair correlation functions, angular distribution functions, densities, coordination numbers and self-diffusion coefficients are compared with published experimental and *ab initio* results for a number of temperatures above the liquidus. Prevalent local orderings are characterized by means of Voronoi analysis. Densities and the temperature coefficient of density are compared with experiment for different compositions of the alloy. All three studied potentials, and EAM-ADP and MEAM in particular, display marked difficulty in describing mixed (Al-Cu) interactions. EAM-ADP mispredicts Cu-rich alloys to re-solidify at all temperatures studied, while MEAM's predictions for the density and its temperature dependence are poor for Al-rich compositions. Overall, the best description of liquid Al-Cu is offered by the Gupta potential, which is found to give a reasonable picture of short-range order and predicts mass transport coefficients and densities in moderately good agreement with experiment.

Keywords: molecular dynamics, Al-Cu alloys, empirical potentials, transferability
PACS: 02.70.Ns, 61.20.Ja, 61.25.Mv

1. Introduction

Aluminum alloys are ubiquitous. Owing to their low density, good forgeability and high thermal conductivity, they are used extensively in the aircraft industry [1], both as bulk structural materials (fuselage frames, chassis), and for high-performance mechanical parts and devices (engine cylinder heads and impellers, propellers, hydraulic systems) [2]. A high yield-strength-to-density ratio, low corrosibility and weldability contribute to their prevalence in shipbuilding (hulls, deckhouses, bilges, tanks) [3] and, coupled with high temperature resistance, in the automotive industry (engine cylinder blocks, truck frames, suspension struts) [4, 5].

Email address: wisnia@kdm.task.gda.pl (Szymon Winczewski)

The addition of copper as main alloying element can serve to improve the hardness and strength of an aluminum alloy through precipitation hardening [4, 6]. High-strength Al-Cu alloys thus find applications in aerospace engineering [7], and their high fracture toughness and resistance to crack propagation are desirable in the construction of light-weight armoured systems [8, 9].

The thermophysical properties of the melt from which Al-Cu alloys are obtained and the conditions under which solidification proceeds in an undercooled alloy fundamentally influence the resultant structure of the solid alloy [10]. A number of experimental investigations of the solidification of Al-Cu shed light on how the microstructure depends on the solidification rate (e.g. Ref. [5]) and how it is influenced by dynamical processes on the microscale (e.g. melt convection [6]). However, a thorough atomic-scale understanding of solidification in Al-Cu alloys remains elusive, as scattering and diffraction experiments lack necessary atomic-level resolution [11].

Another route to the elucidation of structure and dynamics of liquid Al-Cu is through atomic-scale computer simulation. Classical particle-method (molecular dynamics (MD) and Monte Carlo (MC)) simulations of metallic systems enjoy a steady gain in popularity since the introduction of many-body empirical potentials (sometimes referred to as pair functionals [12]) in the 1980s. Most notable examples include the Gupta potential [13], the Finnis-Sinclair model [14], the Sutton-Chen potential [15–17], the effective medium theory (EMT) approach [18, 19], Ercolessi's glue potential [20] and the embedded atom method (EAM) [21–23]. The above-mentioned "metal" potentials all set out to describe metallic bonding by including a local volume or density dependence [24], thereby circumventing known deficiencies of simple pair potentials, such as poorly predicted vacancy formation energies and mispredicted isotropy of elastic constants [12].

Direct application of atomic-scale simulations to dynamical processes (nucleation, diffusion, quenching, age hardening, crack propagation) that are of interest in Al-Cu alloys face a number of considerable difficulties. The limited (sub-μs) timescales accessible to MD calculations pose problems in simulating processes that require statistical averaging of long trajectories, such as melting or re-crystallization [25, 26]. Such simulations, out of sheer necessity, employ heating or cooling rates in the order of 10^{11} K/s or higher [11], far in excess of experimental values. In model calculations time-dependent nucleation effects have been observed to lead to nucleation rates that are orders of magnitude off compared to experiment [27]. Finite-size effects, a consequence of length-scale limitations of atomic-scale simulations, also lead to uncertainties regarding the convergence of obtained results with respect to the size of the simulation cell [27]. Finally, and perhaps most importantly, all empirical potentials assume particular functional forms as models of the electronic interactions that are not accounted for explicitly in classical methods. This is known to lead to their poor transferability, i.e. empirical potentials give qualitatively wrong predictions when they are confronted with phases they have not been parameterized for. Occasionally even common structures pose unexpected difficulties for seemingly reasonably-transferable potentials (see Refs. [28, 29] for discussion).

All the above difficulties notwithstanding, some ambitious efforts have been undertaken very recently in the field: Yanilkin *et al.* [7] studied dislocation mobility in Al-Cu alloys under load, and Singh *et al.* [30] examined the interactions of dislocations with precipitates known to occur in age-hardened Al-Cu alloys. The fact that both of these investigations had to resort to multiscale modeling to properly describe the relevant phenomena serves to illustrate difficulties faced by direct application of MD to the study of dislocation dynamics in these systems.

Some computational efforts have been devoted to the study of the liquid metallic state either for pure Al and Cu [31], or for alloys containing Cu [32, 33]. The only computational study of liquid Al-Cu is due to Wang *et al.* [34], who give insight into the structure of liquid Al-Cu from *ab initio*-driven molecular dynamics, their results compare favourably with experimental results, where these are available. An overview of approaches for calculating thermophysical properties of undercooled alloys and a discussion of limitations of both experimental and computational approaches is given by Lv *et al.* [10]. Morris *et al.* [29] give a short summary of challenges faced by atomic-scale simulations of alloy melts, including an observation that inhomogeneities in the melt can apparently persist well above the eutectic temperature.

Another reason why metallic alloys pose considerably more difficulties for computer simulation compared to pure metals, is due to the complexities of the unlike-atom interactions that are often crucial for correctly modeling chemical ordering. It is not always obvious how to consistently treat these "mixing" interactions [28, 35], which are precisely the interactions that usually play a crucial role in metallic [30] and non-metallic

[36] binary systems alike. A systematic approach in the form of a composition-dependent potential for treating mixed systems has been proposed [37].

The difficulties associated with poor transferability of empirical functional forms can be overcome by using *ab initio* MD (AIMD), whereby electronic effects are modeled directly through explicitly considering the electronic wavefunction (e.g. Hartree-Fock, HF), its radically simplified expansion in terms of atomic orbitals (tight-binding), or the electronic density (density-functional theory). Such approaches require a significantly larger computational effort compared to empirical potentials, and usually scale unfavourably ($O(N^3)$ or worse) with system size. This, in turn, necessitates the use of radically small simulation cells and short timescales, exacerbating the finite-size [27] and finite-time [26, 29] artifacts.

With the above points in mind, it is no surprise that considerable effort is being expended into improving upon existing potentials – by seeking new parameterizations through fits to *ab initio*-derived properties (e.g. Ref. [25]), by identifying and including physically relevant components missing from the description (such as long-range forces [38] in standard EAM), or by generalising existing formalisms to include angular dependence (modified EAM (MEAM) or EAM-ADP potentials) [1, 35, 39, 40], and second-nearest-neighbor effects [28] (2NN-MEAM).

Although newly-developed potentials are usually diligently tested by comparing selected properties with experiment or with *ab initio* calculations, the scope of such tests is typically limited to structures and properties that are of interest to the group developing the potential. How well, or whether at all, the potential transfers to other structures or phases and reproduces different properties is not typically assessed.

The aim of this work is to compare the predictions of three markedly distinct potentials for the Al-Cu system with available experimental and *ab initio* data. In this paper we focus entirely on the liquid state, anticipating future work devoted to the simulation of quenching in the Al-Cu system, for which a reliable description of the initial liquid state will be indispensable.

The paper is organized as follows. In Section 2 we briefly review available experimental and *ab initio* data that were available to us as references to compare against. We devote Section 3 to a more detailed description of the three potentials that we set out to compare. Section 4 summarizes the details of the set-up of our simulations. Results are presented in Sec. 5, while Section 6 is devoted to conclusions.

2. Reference data

We now turn to the justification of the choice of experimental and *ab initio* data that we used to compare the empirical potentials against. Experimental data on Al-Cu alloys that would be directly usable for comparison against computer simulation is admittedly scarce. Below we list relevant experimental work, with a rationale for using, or not, particular results as experimental reference in this work.

Mass transport properties of liquid Al-Cu have been investigated recently – with Brillo *et al.* [41] and Plevachuk *et al.* [42] reporting viscosity measurements, while quasi-elastic neutron scattering (QNS) [41, 43] and cold neutron inelastic scattering [44] have been used, with varying success, to measure the dependence of the self-diffusion coefficient, D, on temperature. The significant scatter (in excess of 50%) in reported experimental values of the self-diffusion coefficient for Al-Cu has been blamed on non-negligible fluid flow in the liquid (an excellent review of available results and a detailed analysis of experimental difficulties is given by Lee *et al.* [45]), at the same time model assumptions used to derive $D(T)$ from QNS data are disputed [41, 43]. Time-resolved X-ray radiography has been used to derive interdiffusion coefficients in Al-Cu melts [46]. These uncertainties in the experimental determination of the self-diffusion coefficient are too large to allow meaningful comparisons of $D(T)$ between simulation and experiment.

Electrical conductivity (measured by Plevachuk *et al.* [42]) is not accessible to classical molecular dynamics simulations.

Viscosities reported by Plevachuk *et al.* [42] are valuable; however, we found through repeated numerical experiments that obtaining sufficiently-converged viscosities from simulations is next to impossible for the Al-Cu system, regardless of employed formalism, due to extremely long correlation times.

Only two sets of experimental data could be reliably compared against simulation – total pair correlation functions obtained from XRD, reported by Wang *et al.* [34] for a single alloy composition, and density and its temperature dependence [42, 47] for a variety of compositions. We used both as reference.

With bleak prospects for comparison against experiment, we include in our reference set the *ab initio* results reported by Wang *et al.* in Ref. [34]. These results were obtained using the plane-wave formulation of DFT, employing Vanderbilt ultrasoft pseudopotentials. Although a number of simplifications were employed (using Γ-point sampling only, using local-density approximation (LDA) for exchange-correlation) and the time- and length-scales (cell sizes) were necessarily limited, Wang *et al.* were diligent in verifying that their results were well-converged with respect to the size of the system, and, crucially, compared the total pair correlation function against high-energy synchrotron XRD experiments, demonstrating excellent agreement. While the fact that total pair correlation functions agree does not conclusively prove that the above DFTMD results are accurate, it provides very strong support for these calculations. The wide spectrum of reported results (total and partial pair correlation functions, angular distribution functions, results of Voronoi tesselation analysis) is also to our advantage, as these properties are readily comparable against classical molecular dynamics simulations. For these reasons we chose to the use results of Ref. [34] as main reference values in this work.

For the sake of making the test as stringent as possible, we endeavour to compare a diverse set of properties – densities and their temperature coefficients for a number of alloy compositions; mass transport properties (diffusion coefficients and their temperature dependence), and the short-range order of $Al_{60}Cu_{40}$, which we will study in detail through the examination of pair correlation functions, angular distribution functions, coordination numbers and species-resolved Voronoi analysis.

3. Potentials studied in this work

We carefully selected three potentials for study, with each representing a distinct class of approaches, and their functional forms differing markedly. The Gupta potential constitutes the simplest of the three descriptions; however, it has a remarkably solid theoretical basis. The parameters for mixed interactions were obtained using customary mixing rules, with no dedicated parameterization of the mixed interactions. This potential does not include angular terms. The EAM-ADP potential, with its explicit inclusion of angular dependence, can be regarded as a model of moderate complexity. Crucially, it is a strongly-dedicated potential, with a parameterization oriented towards reproducing the θ and θ' phases of Al-Cu alloys. The MEAM potential is characterized by the highest degree of complexity. It too is angular-dependent, and, additionally, the energy is calculated with regard to a reference structure. The properties of binary Al-Cu compounds were explicitly used in its parameterization. Compared to EAM-ADP, it is meant as a more general potential.

We follow with a more detailed description of each of the potentials and the parameterizations used in this work.

3.1. Gupta potential

The Gupta potential [13] is a relatively simple many-body potential based on the second-moment approximation to tight binding [48, 49]. The cohesive energy per atom is obtained as a sum of two contributions – an attractive band term E_i^{B}, and a repulsive term E_i^{R}, with the total cohesive energy E_{c} of the system of N atoms given by

$$E_{\mathrm{c}} = \sum_{i}^{N} \left(E_i^{\mathrm{B}} + E_i^{\mathrm{R}} \right) . \tag{1}$$

Gupta derives the band term by assuming the density of states to be represented by a step function and by considering d electrons only. All d-d overlap and transfer integrals are subsequently neglected for second and higher neighbors. The exponential dependence of the transfer integrals follows that of Friedel [48] and Ducastelle [50]. In a further simplification it is assumed that the the s-d contribution, if not negligible, can be approximately accounted for by a suitable rescaling of the nearest-neighbor d-d term. Under the above

assumptions the contribution to the band term from atom i takes the form

$$\begin{aligned} E_i^{\mathrm{B}} &= -\left(\xi_{s_i}^2 \sum_{j\neq i} \rho_j(r_{ij})\right)^{1/2} \\ &= -\left(\xi_{s_i}^2 \sum_{j\neq i} \exp\left(-2q_{s_j s_j}\left(\frac{r_{ij}}{r^0_{s_j s_j}} - 1\right)\right)\right)^{1/2}, \end{aligned} \tag{2}$$

where ξ, q, and r_0 are adjustable parameters, and the sum over j can be identified with the electronic density associated with atom i. A dependence of the parameters on the chemical species of atoms i and j is indicated with subscripts s_i and s_j respectively.

The repulsive potential, which in the underlying tight-binding picture arises from the intersite hopping integrals, is represented by a Born-Mayer repulsive term:

$$\begin{aligned} E_i^R &= \sum_{j\neq i} \phi_{ij}(r_{ij}) \\ &= \sum_{j\neq i} A_{s_i s_j} \exp\left(-p_{s_i s_j}\left(\frac{r_{ij}}{r^0_{s_i s_j}} - 1\right)\right), \end{aligned} \tag{3}$$

where A is a further adjustable parameter.

The values of the parameters are typically determined by fitting to the bulk equilibrium distance, elastic constants and cohesive energies [51, 52]. In this work we use the Al and Cu parameters proposed by Cleri and Rosato [53]. The parameters for mixed (Al-Cu) interactions were obtained using well-known Lorentz-Berthelot mixing rules (A_{AlCu} was obtained as a geometric mean, and p_{AlCu} and r^0_{AlCu} were obtained as arithmetic means of the respective single-species parameters). Note that the contribution of atom j to the electronic density at the site of atom i was taken to depend only on the species of j – hence the pair of subscripts $s_j s_j$ in (2). It was thus not necessary to determine mixed parameters ξ_{AlCu} or q_{AlCu}. Under such description the potential has 13 parameters, these are given in Table 1.

Parameter	Al-Al	Al-Cu	Cu-Cu
A (eV)	0.1221	0.10217496	0.0855
ξ (eV)	1.3160	N/A	1.224
p	8.612	9.786	10.960
q	2.516	N/A	2.278
r_0 (Å)	2.8637	2.70985	2.5560

Table 1: Parameters of the Gupta potential used in this work.

The Gupta potential has been used to study a variety of systems, among these: nanoclusters (Pb [54], Zn [54] and Cd [55], Na [56], Pt [24], Ni [57], Pd [57], Au [57, 58], Ag [57]), where it occasionally proved problematic [57]; surfaces [59], where for Ag it was found to give more realistic predictions compared to EAM; liquid and amorphous metals [60]; and systems with non-trivial competition between hcp and bcc phases (e.g. Zr [61], where it successfully reproduced thermal expansion and phonon dispersion curves).

We did not encounter examples of the use of the Gupta potential to model the Al-Cu system in the literature. Our preliminary calculations indicated its good ability to reproduce the experimental dependence of density on temperature for Al and Cu in the high-temperature region that is of interest in this work. We chose to study the Gupta potential in the hope that it would offer a reasonable description of other thermodynamical propreties of the liquid Al-Cu system.

3.2. EAM-ADP potential

The angular-dependent variant of the embedded-atom method (EAM-ADP) was proposed by Apostol and Mishin [1] in 2011. In this model the total potential energy of the system is given by

$$\begin{aligned} E_{\text{tot}} &= \frac{1}{2}\sum_i \sum_{j\neq i} \phi_{s_i s_j}(r_{ij}) + \sum_i F_{s_i}(\overline{\rho}_i) \\ &+ \frac{1}{2}\sum_{i,\alpha} (\mu_i^\alpha)^2 + \frac{1}{2}\sum_{i,\alpha,\beta} \left(\lambda_i^{\alpha\beta}\right)^2 - \frac{1}{6}\sum_i \nu_i^2, \end{aligned} \tag{4}$$

where

$$\overline{\rho}_i = \sum_{j\neq i} \rho_{s_j}(r_{ij}). \tag{5}$$

The indices i and j denote atoms, while s_i and s_j correspond to their atomic species (Al or Cu). The superscripts α, $\beta \in \{1, 2, 3\}$ denote Cartesian directions. The quantities μ_i^α and $\lambda_i^{\alpha\beta}$ are given by

$$\mu_i^\alpha = \sum_{j\neq i} u_{s_i s_j}(r_{ij}) r_{ij}^\alpha, \tag{6}$$

and

$$\lambda_i^{\alpha\beta} = \sum_{j\neq i} w_{s_i s_j}(r_{ij}) r_{ij}^\alpha r_{ij}^\beta, \tag{7}$$

while ν_i is the trace of $\lambda_i^{\alpha\beta}$, i.e.

$$\nu_i = \sum_\alpha \lambda_i^{\alpha\alpha}. \tag{8}$$

The interpretation of the first two terms in (4) is the same as in the original EAM. As these terms describe the behavior of the individual alloy components in isolation, the functional forms chosen by Apostol and Mishin for ϕ_{AlAl}, ϕ_{CuCu}, ρ_{Al}, ρ_{Cu}, $F_{\text{Al}}(\overline{\rho})$ and $F_{\text{Cu}}(\overline{\rho})$ correspond to those already determined by Mishin *et al.* for pure Al [62] and pure Cu [63].

The remaining three terms in (4) exhibit a non-radial character and serve to describe the effects resulting from the mixing of Al and Cu, that is the varying chemical character in an alloy. These terms significantly affect the energetics of non-cubic phases of Al-Cu. Apostol and Mishin admit that there is no rigorous physical justification for the form of these terms; rather the terms in question were added to introduce an angular dependence and, thereby, to increase the flexibility of the EAM description.

For like pairs of atomic species the functions u and w in (6)-(7) vanish, i.e.:

$$u_{\text{AlAl}}(r_{ij}) \equiv 0, u_{\text{CuCu}}(r_{ij}) \equiv 0, \tag{9}$$

and

$$w_{\text{AlAl}}(r_{ij}) \equiv 0, w_{\text{CuCu}}(r_{ij}) \equiv 0. \tag{10}$$

The cross-functions u_{AlCu} and w_{AlCu}, and the form of ϕ_{AlCu} were parameterized through fitting to experimental and *ab initio* results. The quantities fitted included the energies of formation of the eight most significant phases of Al-Cu and the structural (lattice constants) as well as mechanical properties (elastic constants) of the θ i θ' phases. This makes ADP an ideal candidate for studying precipitation hardening in Al-Cu alloys.

Since its inception, the ADP potential has been used in studies of the dynamical properties of dislocations in Al-Cu alloys [7], to study the mechanisms of motion of dislocations through Guinier-Preston (GP) zones [7], in molecular-dynamics simulations that served as base for a hierarchical multiscale model for studing aging and hardness in precipitation-hardened Al-Cu alloys [30], and in a study of diffusion bonding of the Al-Cu interface [64].

3.3. MEAM potential

In the modified embedded-atom method (MEAM) [65, 66] approach, the total potential energy of the system is given by

$$E_{\mathrm{tot}} = \frac{1}{2}\sum_i \sum_{j\neq i} \phi_{ij}(r_{ij}) + \sum_i F_i(\overline{\rho}_i). \tag{11}$$

The interpretation of both terms is the same as for the original EAM. The embedding energy is given by

$$F_i(\overline{\rho}_i) = \begin{cases} A_{s_i} E^0_{s_i} \overline{\rho}_i \ln(\overline{\rho}_i) & \text{for} \quad \overline{\rho}_i \geq 0, \\ -A_{s_i} E^0_{s_i} \overline{\rho}_i & \text{for} \quad \overline{\rho}_i < 0. \end{cases} \tag{12}$$

In (12), the sublimation energy E^0 and the parameter A are subscripted with s_i, which serves to remind the Reader that these quantities depend on the atomic species.

The background electronic density is given by

$$\overline{\rho}_i = \frac{\rho_i^{(0)}}{\rho_i^0} G(\Gamma_i), \tag{13}$$

where

$$G(\Gamma) = \begin{cases} \sqrt{1+\Gamma} & \text{for} \quad \Gamma \geq -1, \\ -\sqrt{|1+\Gamma|} & \text{for} \quad \Gamma < -1. \end{cases} \tag{14}$$

The function Γ_i is given as a sum

$$\Gamma_i = \sum_{k=1}^{3} t_i^k \left(\frac{\rho_i^{(k)}}{\rho_i^{(0)}} \right), \tag{15}$$

where $\rho_i^{(k)}$ are partial electronic densities of zero and higher orders. The assumption of the above form for the electronic density is what markedly distinguishes the MEAM model from other EAM-like descriptions. The quantity ρ_i^0 plays the role of a scaling factor, defined by the choice of a reference structure. The partial electronic densities of higher orders serve as correction terms, taking into account the changes in the electronic density resulting from the deviation of the character observed in the local environment of atom i from that of the reference structure. The correction terms vanish for the cubic case (chosen as reference). All the contributions to the density $\overline{\rho}_i$ display a marked local character, depending only on the position of atom i and of its nearest neighbors (1NN-MEAM model). The inclusion of the second coordination shell gives rise to the so-called 2NN-MEAM models [67, 68].

The distinct character of the MEAM potential is also apparent from the construction of the pairwise term, which is given by

$$\phi_{ij}(r_{ij}) = \overline{\phi}_{ij}(r_{ij}) S_{s_i s_j}. \tag{16}$$

In the above expression the quantity $S_{s_i s_j}$ represents the so-called screening function, whose form is more general than a two-body (pairwise) term. The subscripts $s_i s_j$ only serve to indicate its dependence on the species of atoms i and j. The screening function is constructed in such a way that it assumes a value of 1 when atoms i and j are not screened and are within the cutoff distance, and a value of 0 when atoms i and j are fully screened or are further away than the cutoff distance. The role of the screening function is to modulate pairwise interactions, enforcing their smooth truncation.

The form of $\overline{\phi}_{ij}(r_{ij})$ is atypical too, with a dependence on the coordination numbers Z_i and Z_j of atoms i and j. Crucially, this quantity is also calculated with regard to a reference structure, similarly to the manner in which this has been done for $\overline{\rho}_i$. Due to the complexity of the expressions for $\overline{\phi}_{ij}(r_{ij})$, $S_{s_i s_j}(r_{ij})$, ρ_i^0, $\rho_i^{(0)}$ and $\rho_i^{(k)}$ and t_i^k (where $k \in \{1,2,3\}$), they will not be given in full in this work. For details the Reader is referred to e.g. Ref. [35].

The flexibility of the MEAM model allows it, in principle, to be highly transferable. By virtue of being able to automatically switch the forms used to calculate the embedding energy and the energy of pairwise interactions, MEAM potentials set out, in the framework of a single formalism, to correctly reproduce the

properties of a number of distinct phases, including structures as distinct as bcc and hcp (even with non-ideal c/a ratios) [66], and to describe systems generally considered difficult, such as Zr or Ti [69].

In 2012 Jelinek *et al.* [35] presented a 1NN-MEAM type potential for aluminum, silicon, magnesium, copper and iron. This potential has been based on potentials available for pure elements, with formation energies of stable binary compounds obtained from *ab initio* calculations used in the parameterization. According to the authors, this potential should correctly describe binary or ternary systems of the component elements (Al, Si, Mg, Cu and Fe). We were unable to find applications of this potential to the Al-Cu system in the literature (yet). However, having in mind the strengths of the MEAM approach (transferability resulting from self-adaptability), we chose the potential of Jelinek *et al.* as one of the descriptions to be tested in this work.

4. Computational details

We focus entirely on the liquid state. We devote most of our attention to $Al_{60}Cu_{40}$, for which, we believe, reliable reference results can be obtained from Ref. [34]. The choice of reference data dictates, in turn, the temperatures we studied (973 K to 1323 K, with a step of 50 K). For other alloy compositions we compare against the experimental results of Plevachuk *et al.* [42], sampling a temperature range of 1000 K. . . 1300 K, again with a step of 50 K.

All simulations in this work employ molecular dynamics, with all presented results sampling the NpT ensemble, at zero external pressure. Temperature and pressure were controlled using a Nosé-Hoover [70–72] thermostat in the formulation of Shinoda [73]. Average temperatures during sampling were found to lie within 1 K of the target temperature, with a standard deviation of 10-20 K. Velocity rescaling was used only during equilibration.

Our detailed protocol is as follows. We began with equilibration at 2500 K for 50 ps, where velocity rescaling was applied simultaneously with temperature and pressure control. At this stage velocity rescaling was turned off, and the system was kept at 2500 K for a further 250 ps to ensure homogeneity, using only the thermo- and barostat. Each system was subsequently cooled to the target temperature at a rate of 1 K/ps, and then equilibrated (in the absence of velocity rescaling) for a further 50 ps. This was followed by sampling over 250 ps at the target temperature. The variations in the dimensions of the simulation cell were monitored to ensure that no atom ever self-interacted with its own periodic images. All calculations were performed with the LAMMPS [74] package, using a timestep of $\Delta t = 1$ fs.

Initial configurations at the mixing temperature $T = 2500$ K were generated as fcc crystals. Each system comprised 4000 atoms, with the species (Al or Cu) of each atom in the fcc lattice randomized. Periodic boundary conditions were used. Densities d were determined from linear relationships for densities of pure Al and Cu in the liquid state as a function of temperature:

$$d(T) = d_{\mathrm{m}} + d_{\mathrm{T}}\,(T - T_{\mathrm{m}})\,, \tag{17}$$

where d_{m} is the density at the melting temperature T_{m}, and d_{T} is the temperature coefficient of density. Following Ref. [75] we used the following values: $d_{\mathrm{m}}^{\mathrm{Al}} = 2.375$ g cm^{-3}, $d_{\mathrm{T}}^{\mathrm{Al}} = -2.33 \times 10^{-4}$ g cm^{-3} K^{-1}, $T_{\mathrm{m}}^{\mathrm{Al}} = 933.47$ K, $d_{\mathrm{m}}^{\mathrm{Cu}} = 8.020$ g cm^{-3}, $d_{\mathrm{T}}^{\mathrm{Cu}} = -6.09 \times 10^{-4}$ g cm^{-3} K^{-1}, $T_{\mathrm{m}}^{\mathrm{Cu}} = 1357.77$ K. Ideal mixing was assumed for the determination of the initial density:

$$\widetilde{d}_{\mathrm{AlCu}}(x,T) = (1-x)\,\widetilde{d}_{\mathrm{Al}}(T) + x\,\widetilde{d}_{\mathrm{Cu}}(T), \tag{18}$$

where $\widetilde{d}$ correspond to atomic densities, and x is the atomic content of Cu. We reiterate that the above procedure was only used to generate initial configurations, and the system was allowed to relax through the use of the NpT ensemble with zero external pressure. The same procedure was used in the reference calculations by Wang *et al.* [34].

The potentials used in this work differ not only with regard to their construction, but also with regard to the employed cutoff radius. For the EAM-ADP and MEAM potentials the cutoff radius is dictated by the model, i.e. it has been determined during the parameterization of the potential. For the EAM-ADP

potential the cutoff radius is 6.28 Å, while for the MEAM potential it is 5.0 Å. This is not to say that these potentials are short-ranged, with no interactions between atoms separated by more that several Å – one has to keep in mind that the actual interaction range is longer due to the presence of the many-body term that introduces coupling between neighbors of neighbors. For the Gupta potential one is free to choose the cutoff radius. In this work Gupta interactions were truncated to zero at 12.0 Å using a smooth cutoff whereby both $\phi_{ij}(r)$ and $\rho_i(r)$ were smoothly truncated using a cutoff-function of the form

$$f_{\mathrm{c}}(r) = \begin{cases} 1 & \text{for} \quad r < r_{\mathrm{m}} - r_{\mathrm{d}}, \\ \frac{1}{2} - \frac{1}{2}\sin\left(\frac{(r-r_{\mathrm{m}})\pi}{2r_d}\right) & \text{for} \quad r_{\mathrm{m}} - r_{\mathrm{d}} \leq r \leq r_{\mathrm{m}} + r_{\mathrm{d}}, \\ 0 & \text{for} \quad r > r_{\mathrm{m}} + r_{\mathrm{d}}, \end{cases} \tag{19}$$

with $r_m = 11$ Å and $r_d = 1$ Å for all pairs: Al-Al, Al-Cu, and Cu-Cu.

Calculations for each temperature and each potential were repeated three times (with randomness imbued by the selection of initial velocities) to give insight into the repeatability of results. All presented results represent averages over the three sets of runs, unless indicated otherwise.

5. Results

5.1. Pair corellation functions

We begin with a comparison of pair correlation functions for four temperatures: 1023 K, 1123 K, 1223 K, and 1323 K, all of which lie above the liquidus point for $Al_{60}Cu_{40}$. Results obtained by Wang *et al.* [34] from DFTMD calculations are in excellent agreement with experimental data, particularly for lower temperatures. For higher temperatures the DFTMD calculations overestimate the height of the first peak to a small degree.

Fig. 1 compares the experimental and *ab initio* results of Ref. [34] with our calculations using the three empirical potentials. Of course only total pair correlation functions are accessible to experiment. Moderate agreement is observed in total pair correlation functions for the Gupta and MEAM potentials, both of which somewhat overestimate the nearest-neighbor distance and the height of the first peak, with the Gupta potential yielding better agreement with experiment and DFTMD results for the first peak, and MEAM yielding moderately better agreement for the second peak (where both potentials overestimate its position). The EAM-ADP potential clearly leads to an overstructuring, predicting deep minima, well-pronounced peaks and the presence of an unexpected shoulder at around 4 Å. For the Al-Al pair correlation function (cf. Fig. 1b) only the Gupta potential remains in reasonable agreement with *ab initio* calculations, although it slightly overestimates the positions and heights of both the first and second peak. MEAM clearly mispredicts artificially strong Al-Al interactions, leading to an overestimation of the height of the first peak by as much as 80%, and of the second peak by about 25%, although the positions of both peaks are in good agreement with DFTMD. The predictions of EAM-ADP are similar to those of the Gupta potential for the first peak, while at larger distances a tendency to overstructure again becomes apparent. The situation is similar for the Cu-Cu pair correlation functions (cf. Fig. 1c), where MEAM dramatically overestimates the strength of like (Cu-Cu) interactions, in consequence overestimating the height of the first peak by as much as 200%. The Gupta potential provides, relatively, the best agreement with DFTMD, although it too seems to overestimate the Cu-Cu binding. The results of EAM-ADP disagree entirely. For mixed (Al-Cu) pair correlation functions (cf. Fig. 1d) agreement of each of the empirical potentials with *ab initio* results is poor, with the Gupta potential performing best, reproducing the broad second peak and, to a degree, the first peak. MEAM underestimates the strength of Al-Cu interactions, leading to a diminished and misplaced first peak. ADP-EAM does reproduce the positions of the peaks, but significantly overestimates their heights.

All the three empirical potentials studied have clear difficulty treating mixed interactions in $Al_{60}Cu_{40}$, with the predictions of the Gupta potential encumbered by the smallest errors. We feel obliged to point out that the plane-wave pseudopotential DFTMD description that serves as a reference here can also occasionally suffer from a dependence of the interactions, and thus structures, on the precise pseudopotential used. A comprehensive study of the effect of the pseudopotential (and perhaps the exchange-correlation functional) on the obtained structure would be invaluable, but is outside the scope of this work. Here we were more

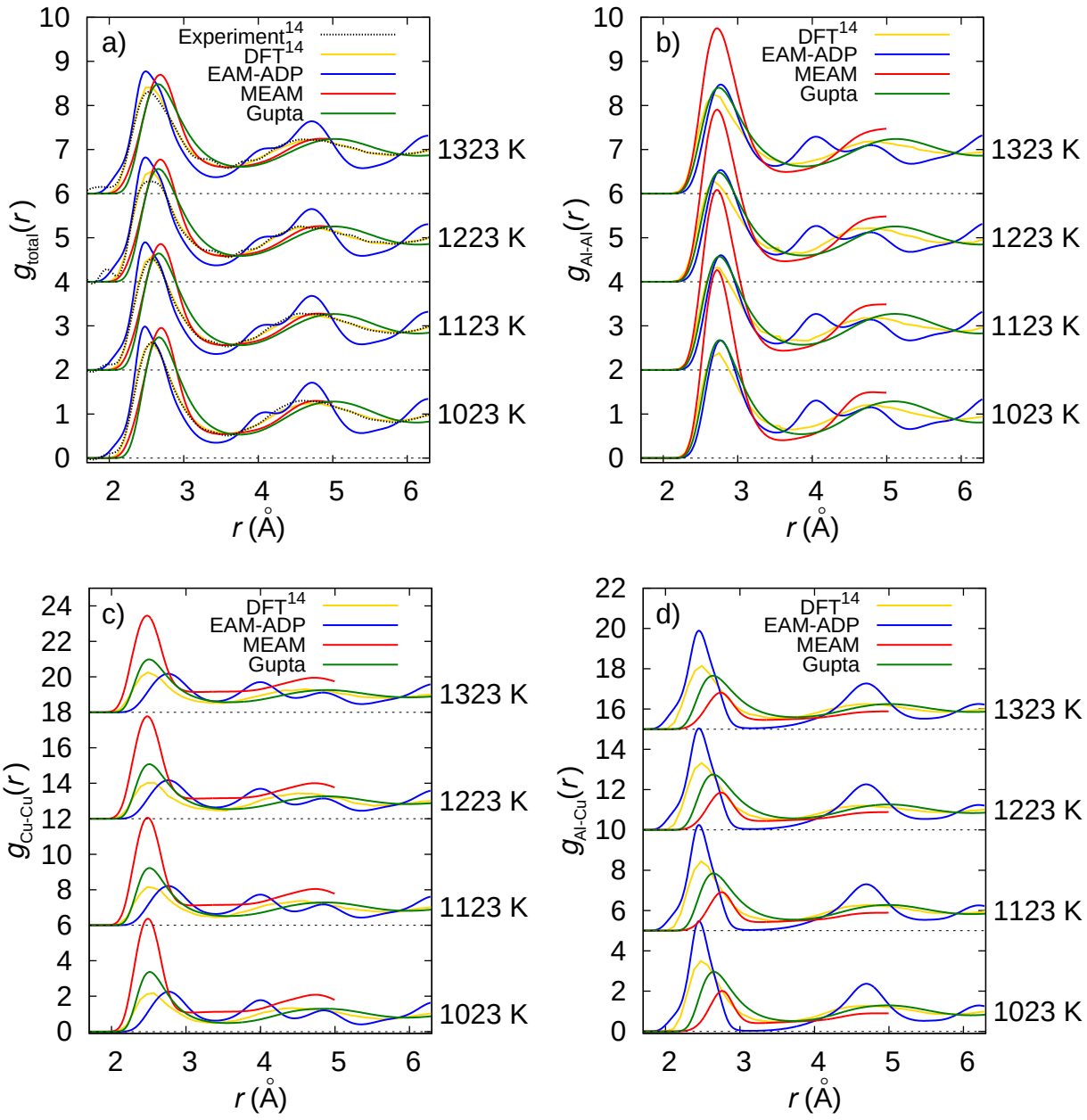

Figure 1: Total (panel a) and partial (panels b-d) pair correlation functions of the liquid $Al_{60}Cu_{40}$ alloy for four temperatures. Values for 1123 K, 1223 K and 1323 K were shifted by an integer number of units, this is indicated with dashed horizontal lines. MEAM results (in red) are truncated at the potential cutoff.

alarmed by the tendency of EAM-ADP to overstructure and felt it warranted further attention. On closer inspection we discovered that the pair correlation functions obtained with this potential for our system were poorly reproducible. This is demonstrated in Fig. 2, where we separately plot the total and mixed (Al-Cu) pair correlation functions obtained from three sets of calculations with differing initial conditions. For a thoroughly equilibrated liquid system we would expect macroscopic properties not to differ appreciably between production runs, and this is indeed the case for the results obtained with the Gupta potential and

the MEAM potential.

5.2. Mass transport properties

To further investigate this issue, we calculated the self-diffusion coefficients of Al and Cu in the alloy using the Einstein relation for the eight temperatures for which they are reported in Ref. [34]. The results are shown in Fig. 3, where we purposefully plot the results of each of the three production runs separately, to demonstrate the reproducibility for the Gupta and MEAM potentials and the dependence on initial conditions seen with EAM-ADP. The extremely low values of the self-diffusion coefficient confirm our suspicions – the EAM-ADP system proceeded to re-solidify in each of our calculations, even for temperatures as high as 1323 K. With the cooling rate obviously insufficiently low for re-crystallization, the three systems became "trapped" in three different local minima. The appearance of this unfortunate effect means that subsequent results obtained with EAM-ADP for $Al_{60}Cu_{40}$ do not correspond to a true liquid state and should not be interpreted as such. Instead, EAM-ADP must be assumed not to be able to describe liquid $Al_{60}Cu_{40}$ below (at least) 1323 K. Further results obtained with this potential will, however, be shown for the sake of completeness. In order to remind the Reader of the above deficiency, subsequent plots will be augmented with error bars to indicate the differences between the three sets of calculations. These differences will generally be seen to be negligible for the Gupta and MEAM potentials and appreciable for EAM-ADP. We will briefly return to the issue of reproducibility in Section 5.5.

We proceed by noting a very good agreement in both the absolute values and the slope of $D(T)$ between the Gupta potential and DFTMD results, and moderate agreement for MEAM, which underestimates the diffusion rate and slightly overestimates the temperature dependence. In all cases the temperature dependence is desribed well by the Arrhenius relation

$$D(T) = D_0 \exp\left(-E_\mathrm{a}/k_\mathrm{B}T\right). \tag{20}$$

We summarize the activation energies E_a and pre-exponential factors D_0 in Table 2.

Approach	E_a^Al (kJ/mol)	D_0^Al (cm^2/s)	E_a^Cu (kJ/mol)	D_0^Cu (cm^2/s)
EAM-ADP	86.9	0.00187	76.4	0.00047
MEAM	61.1	0.00521	43.9	0.00129
Gupta	27.9	0.00084	27.7	0.00079
DFT[34] (reference)	20.6	0.00036	19.7	0.00028

Table 2: Activation energies and pre-exponential factors describing mass transport in $Al_{60}Cu_{40}$.

5.3. Overview of short-range order

We begin our analysis of short-range order in the liquid $Al_{60}Cu_{40}$ alloy by comparing, against the results of Ref. [34], the frequencies with which the most common structural motifs occur. We also briefly compare the ratios of the coordination numbers of Al and Cu atoms. Following Wang *et al.* we employed Voronoi tesselation[76] as a means of structure identification. When applied to liquid systems, Voronoi tesselation runs into difficulties related to distinguishing nearest neighbors from second-nearest neighbors. At higher temperatures the presence of second-nearest neighbors, which are instantaneously driven close to the center of the Voronoi polyhedron by thermal motions, leads to the appearance of spurious faces in the polyhedron, which hinders analysis. A popular approach for filtering out second-nearest-neighbor contributions consists in eliminating Voronoi faces with small surface areas. Another, simpler approach relies on using a distance cutoff during tesselation. This approach has been used by Wang *et al.*, with a fixed cutoff of 3.56 Å, corresponding to the first minimum of the total pair correlation function. For the sake of facilitating comparison, in this work we followed an analogous approach. However, since we compare three different potentials, each of which predicts different positions of the first $g(r)$ minimum, it becomes

necessary to introduce some kind of cross-calibration so that the three potentials can be treated on the same footing. We achieved this by tuning the tesselation cutoff length separately for each potential and each temperature such that the *average* geometrical coordination number (i.e. the mean number of faces in the Voronoi polyhedron, following the application of a radial cutoff) was identical to that of Wang *et al.*. Our dependences of average coordination numbers on temperature are thus, for every potential, by construction, identical to those of Ref. [34], Fig. 8a therein.

In Fig. 4 we plot the Al/Cu coordination number ratio predicted by the three potentials under study. Only the Gupta potential agrees with the DFTMD results in predicting that the coordination number of Al is larger than the Cu coordination number, with the reverse prediction made by EAM-ADP and MEAM. All three potentials underestimate this quantity, although the trend of it decreasing roughly monotonically with temperature is correctly recovered. EAM-ADP is again seen to have reached three different "frozen" configurations starting from three different initial conditions.

In Fig. 5 we show the frequency histograms of individual Voronoi polyhedra for $T = 973$ K, where the discrepancies between the predictions of the empirical potentials were the most pronounced. The standard signature notation $\langle f_3, f_4, f_5, f_6 \rangle$ is used, where f_i denotes the number of faces with i edges. Apart from total histograms (panel a), results for Al-centered (panel b) and Cu-centered (panel c) polyhedra are shown. These results are directly comparable to those shown in Fig. 5 of Ref. [34], although we reproduce those reference results in our plot for ease of comparison. We focus on the 12 types of Voronoi polyhedra which are the most abundant in the studied alloy and encompass over 60-70% of all the identified polyhedra, depending on temperature. The same polyhedra were reported by Wang *et al.*, and they are commonly regarded as main structural motifs in liquid metals.

For the sake of brevity we do not present a detailed breakdown for the remaining two temperatures studied by Wang *et al.* (1073 K and 1323 K); however, we discuss the results for these temperatures briefly in terms of an averaged structure description mismatch, a scalar measure defined as

$$m = \sum_{v \in V} \left| \frac{f_v - f_v^{\mathrm{ref}}}{f_v^{\mathrm{ref}}} \right| f_v^{\mathrm{ref}} = \sum_{v \in V} \left| f_v - f_v^{\mathrm{ref}} \right| . \tag{21}$$

Here, with f_v we denote the frequency of the occurrence of polyhedra of type v, with v running through all twelve considered polyhedra types ($\langle 0,2,8,0 \rangle$, ..., $\langle 0,3,6,4 \rangle$). The reference frequency of Ref. [34] is denoted with f_v^{ref}. The measure m can be viewed either as a sum of relative errors, with each term weighted with the corresponding frequency f_v^{ref}, or as a total error of a description, informing about a fraction of atoms for which the predicted local environment is in disagreement with the reference, and thus about how erroneous, in an average sense, the obtained structure is. In Fig. 6 we separately show the values of m for the total structure, and for Al-centered and Cu-centered polyhedra.

Even a cursory glance at Fig. 6, panel a), makes it apparent that the EAM-ADP potential incorrectly describes the short-range order of liquid Al-Cu alloys, with a description mismatch of about 16% for all the three studied temperatues, while for the remaining two potentials m is approximately 11% (for lower temperatures), and as low as 7% for 1323 K. While the species-averaged errors obtained for the MEAM and Gupta potential are comparable, we deem the predictions of the MEAM potential to be significantly worse. This is evidenced by very large errors for Al-centered polyhedra, with a mismatch of approximately 14-15% for 973 K and 1073 K, and 9% for 1323 K, which is more than twice as large as for the Gupta potential. We conclude that, when the heterogeneity of the studied systems is taken into account, the MEAM potential offers a poor description of the local order in liquid Al-Cu, with its low species-averaged mismatch apparently a result of judicious error cancellation between Al-centered and Cu-centered structures. This is easily seen on the example of $\langle 0,2,8,1 \rangle$ polyhedra, whose frequency the MEAM potential significantly overestimates for Al-centered polyhedra (cf. Fig. 5, panel b), while simultaneously significantly underestimating it for Cu-centered polyhedra (panel c therein), resulting in an acceptably low total error (cf. panel a).

The above examination of the structure mismatch allows us to conclude that, out of the three studied potentials, the Gupta potential manages best to reproduce the correct short-range order, being the only potential that simultaneously describes well the local environment of the Cu atoms (m in the order of 9, 8, and 5%), and of the Al atoms (m as low as 7, 6, and 4%). The only deficiency of the Gupta potential

in this context lies in its inability to offer a quantitatively correct description of local icosahedral ordering, with an overestimation of the frequencies of icosahedral and icosahedron-like structures, for both Al- and Cu-centered polyhedra. In Fig. 5 this is manifested in the large heights of bars denoted with $\langle 0,0,12,0\rangle$ (corresponding to icosahedra) and $\langle 0,1,10,2\rangle$ (corresponding to capped icosahedra), as well as $\langle 0,2,8,0\rangle$, $\langle 0,2,8,1\rangle$ and $\langle 0,2,8,2\rangle$ (commonly regarded as Voronoi polyhedra of icosahedron-like structures). We shall denote the set of the above signatures as I. We point out that it is the errors in the frequencies of polyhedra $v \in I$ that are largely responsible for the discrepancy between the description offered by the Gupta potential and the reference descriptors obtained from DFT.

To further the point, in Tab. 3 we juxtapose, for three temperatures, the values of measures characterising the local icosahedral ordering, namely $f_{\mathrm{icos}} = \sum_{v\in I} f_v$, which is a measure of the total frequency of icosahedron-like motifs, and $m_{\mathrm{icos}} = \sum_{v\in I} \left|f_v - f_v^{\mathrm{ref}}\right|$, which measures the error in the description of icosahedral ordering. It now becomes clear, that the error in the description of icosahedral ordering m_{icos} is mainly responsible for the total error m in the Gupta potential's description of the short-range order. We point out that any contribution to m_{icos} can at most (in the worst-case scenario) become twice as large in m, which follows from how the measure m is constructed. The values shown in Tab. 3 demonstrate that the Gupta potential consistently overestimates the tendency towards icosahedral ordering. This can be explained by the spherically-symmetric form of this potential (the function describing the electronic density term), which is expected to favour icosahedron-like structural motifs.

Temperature	f_{icos} (%)		m_{icos} (%)	m (%)
	DFT[14]	Gupta		
		Al-centered		
973 K	16.77	20.58	3.81	6.82
1073 K	15.58	19.06	3.46	6.02
1323 K	14.25	15.84	1.64	3.67
		Cu-centered		
973 K	11.42	15.46	5.01	9.06
1073 K	10.35	13.97	4.19	7.96
1323 K	9.23	11.06	2.32	5.24

Table 3: Measures describing icosahedral ordering obtained for the Gupta potential.

The fact that the Gupta potential overfavours icosahedral structures is also seen from the angular distribution function ADF(Θ) (cf. Fig. 7), where the position of the first maximum is shifted towards the characteristic icosahedron/tetrahedron 60° angle. As a result, the height of the first maximum is also overestimated. Consequently, the position of the second maximum is shifted towards the 108° angle, characteristic for the pentagonal structure also present in an icosahedron, with the height slightly underestimated. Overall, the agreement in ADF(Θ) between the Gupta potential and the reference DFT results remains moderately good, exceeding that of the MEAM potential and of the EAM-ADP potential in particular.

While the species-averaged plots of ADF(Θ) for the MEAM potential appear qualitatively similar to those of the Gupta potential (and thus to the reference DFT results), a more detailed examination of the short-range order based on Voronoi analysis unequivocally demonstrated that this agreement is coincidental, and the structure obtained from the MEAM potential shows more serious discrepancies from the reference when the local environment is examined for each atomic species separately.

In the case of the EAM-ADP potential the agreement in ADF(Θ) with the reference results is very poor, with extraneous maxima being predicted, which correspond to right and straight angles. This is evidence that for the temperature range studied here the EAM-ADP potential strongly overfavours cubical and/or tetragonal motifs, yielding an incorrect description of local ordering.

The above examination of local structure prediction can be summarized by stating that the Gupta potential is the least incorrect in its reproduction of the structural variety of Al-Cu alloys at temperatures

slightly above the liquidus. In the context of its remarkably simple form, the discrepancies of the Gupta potential can be thought of as extraordinarily low.

5.4. Density

We now turn to the last quantity studied in this work – density and its temperature dependence. Our aim was to briefly study how the three potentials of interest describe compositions other than $Al_{60}Cu_{40}$. We compare liquid densities for three compositions for which experimental data due to Plevachuk *et al.* [42] is available – these are 4, 20 and 30 wt pct Cu. We also include a comparison for $Al_{60}Cu_{40}$ (corresponding to Al-61 wt pct Cu) against the DFTMD results of Ref. [34].

We employed the same simulation protocol as for $Al_{60}Cu_{40}$ (mixing at 2500 K, cooling to target temperature at a constant rate, sampling the NpT ensemble at target temperature and zero external pressure). We calculated the density $d(T)$ for seven temperatures $T = 1000, 1050, \ldots, 1300$ K. Like before, we repeated each calculation three times with different initial conditions. The calculated densities and linear fits to their temperature dependence according to (17) are shown in Fig. 8. The results of the fits (predicted densities d_m at melting point, and temperature coefficients d_T of density) are summarized in Table 4.

Alloy	Reference data			EAM-ADP		MEAM		Gupta	
(wt % Cu)	T_m	d_m	d_T	d_m	d_T	d_m	d_T	d_m	d_T
4	922	2.43	-3.20	2.53	-2.47	1.55	5.10	2.49	-2.88
20	873	2.71	-4.05	2.98	-2.99	2.66	-0.67	2.83	-3.25
30	836	2.93	-4.02	3.35	-3.50	3.25	-4.02	3.10	-3.53
61	933	4.33	-2.51	5.19	-1.65	4.37	-6.19	4.24	-4.85

Table 4: Density and its temperature dependence for Al-Cu alloys. The melting temperature T_m is given in K, density at melting point d_m in $\mathrm{g\,cm^{-3}}$, and the temperature coefficient of density d_T in 10^{-4} $\mathrm{g\,cm^{-3}\,K^{-1}}$. For the first three compositions the reference is the experimental work of Plevachuk *et al.* [42], the last composition is compared against DFTMD results of Wang *et al.* [34].

Alloy	EAM-ADP		MEAM		Gupta	
(wt % Cu)	$\left\lvert\frac{\Delta d_\mathrm{m}}{d_\mathrm{m}}\right\rvert$	$\left\lvert\frac{\Delta d_\mathrm{T}}{d_\mathrm{T}}\right\rvert$	$\left\lvert\frac{\Delta d_\mathrm{m}}{d_\mathrm{m}}\right\rvert$	$\left\lvert\frac{\Delta d_\mathrm{T}}{d_\mathrm{T}}\right\rvert$	$\left\lvert\frac{\Delta d_\mathrm{m}}{d_\mathrm{m}}\right\rvert$	$\left\lvert\frac{\Delta d_\mathrm{T}}{d_\mathrm{T}}\right\rvert$
4	4.1%	23%	36%	260%	2.4%	10%
20	9.1%	26%	1.8%	83%	4.4%	20%
30	14%	13%	11%	0%	5.8%	12%
61	20%	34%	0.92%	150%	2.1%	93%

Table 5: Relative error in the calculated diffusion coefficient at melting temperature d_m and in the temperature coefficient of the density d_T. Reference values mirror those of Tab. 4.

We conclude that the Gupta potential is the most accurate in its predicitions for the density of liquid Al-Cu in a broad range of compositions. Typical relative errors (summarized in Table 5) for this potential are in the order of $2-6\%$ (for d_m) and $10-20\%$ (for d_T), with densities slightly overestimated compared to experiment. We note that the errors in the predictions of the Gupta potentials are particularly small for the low-Cu composition, which is of greatest technological significance.

The EAM-ADP potential also overestimates the density, to a larger degree. The errors are roughly twice as big (for d_m) or comparable (for d_T) to those of the Gupta potential. Cu-rich alloys in particular are

poorly described, with errors in the density as large as 20%. We note that the dependence of the structure on the initial condition, previously observed for higher Cu contents, disappears for Al-rich alloys.

The MEAM potential fares particularly badly for Al-rich alloys – for Al-4 wt pct Cu it wildly underestimates densities (d_{m} is 36% off) and predicts a reverse trend for the temperature dependence. Also worrying is its tendency for the predictions to vary between calculations which differed only with regard to the initial conditions. This is evidenced a spread in the diffusion coefficients obtained from three different runs (cf. Fig. 8, panels a and b). Indeed, below 30 pct wt Cu MEAM predicts an unphysical spontaneous solidification of the alloy into a foam-like structure containing relatively large voids surrounded by several-atom-thick filaments (cf. Fig. 9), with a roughly uniform distribution of Cu atoms. The result is disastrously low density and a reverse prediction for the dependence of density on temperature. We presume that the flexible, auto-switching form of this potential leads to unphysicalities for disordered systems with highly-variable local chemical composition. Our results indicate that the transferability of this potential to liquid systems is severely limited and it is not a good candidate for studying liquid Al-Cu. We note that with increasing Cu content the predictions of the MEAM potential improved, and the above artifacts were no longer present.

5.5. Reproducibility of results

We now briefly return to the issues of reproducibility of the obtained results, with particular focus on the behavior of the EAM-ADP potential at low temperatures. In previous sections we have already highlighted the significant scatter in results for all the studied properties for EAM-ADP, in contrast to very good reproducibility achieved with the Gupta and MEAM potentials for the $Al_{60}Cu_{40}$ system. Referring to the extremely low values of the diffusion coefficient predicted by EAM-ADP (cf. Fig. 3) we proposed to explain these surprising results by a spurious re-solidification of the alloy, each time to a different local energy minimum. Below we strengthen our explanation by examining the caloric curve for the cooling process for the three studied potentials, which we present in Fig. 10.

The dependence of total energy on temperature is seen to be linear for the Gupta potential and almost linear for the MEAM potential, indicating the absence of a phase transition. Moreover, the curves corresponding to different initial conditions overlap almost ideally, demonstrating that these potentials generate reproducible liquid states.

In the case of the EAM-ADP potential we observe a change in the slope of $E_{\mathrm{tot}}(T)$ between 1500 K and 1250 K, which is indicative of a structural change. Careful examination reveals that at this temperature range the system gradually transitions from a liquid to a solid state. The employed cooling rate is such that the observed structural change corresponds neither to a pure crystallization nor to typical glassification. What is more, the resultant structure does not resemble any typical phase of Al-Cu, and is different for each set of initial conditions. This observation is supported by the variation in the measures of structural order seen in Figs. 1, 2, 4 and 5, and the caloric curves shown in Fig. 10. The caloric curves corresponding to different initial conditions become considerably distinct below 1500 K, with energy differences of almost 0.04 eV/atom at 973 K.

6. Conclusions

The predictions of three empirical many-body potentials were compared with *ab initio* results and experiment for liquid Al-Cu alloy systems of various compositions. Each of the potentials struggled to correctly reproduce the correct picture of local ordering, which confirms the notion that liquid metallic alloys constitute difficult systems.

EAM-ADP mispredicted the $Al_{60}Cu_{40}$ alloy to solidify at all studied temperatures (up to 1323 K), despite the fact that the melting temperature of this alloy is 933 K [34], with self-diffusion activation energies overestimated approximately fourfold. Consequently, the predicted short-range order was poorly described, both in the vicinity of Al and Cu atoms, with cubic ordering strongly overfavoured; the tendency for Al-Cu pairing in the first coordination shell was overestimated, with Al-Al and Cu-Cu pairing overestimated in the second shell. The densities obtained for Cu-rich alloys were in particularly poor agreement with experiment,

with errors as large as 20%. To give justice to EAM-ADP, we point out that this potential was designed to study precipitation hardening, thus focusing mainly on the correct description of the stability of θ and θ' phases and not on the liquid phase.

The MEAM potential correctly predicted $Al_{60}Cu_{40}$ to be in the liquid phase for the temperatures studied. Mass transport properties were in qualitative, but not quantitative agreement with DFT results, with self-diffusion activation energies overestimated by a factor of 2.2 for Cu and threefold for Al. This potential had marked difficulty in correctly capturing the chemical ordering of the alloy – the strength of Al-Al and Cu-Cu interactions was dramatically overestimated, which was evidenced by the heights of the first maxima in the corresponding partial pair correlation functions being radically (sometimes by a factor of 3) larger than the reference values. The same difficulties, e.g. a particularly poor description of local order in the vicinity of Al atoms, were exposed by species-resolved Voronoi analysis. Even with the above discrepancies, the species-averaged picture of the structure and dynamical properties of $Al_{60}Cu_{40}$ were in better agreement with DFT, compared to EAM-ADP. However, as the composition of the alloy was varied, the MEAM potential could not correctly describe alloys with low Cu content.

The Gupta potential, despite its conceptual simplicity, performed the best out of the three potentials. Mass transport properties were in good agreement with DFT results (activation energies overestimated by 40%). Pair correlation functions, although far from ideal, were closest to those obtained from DFT and experiment. Out of the three potentials it was the only one to display a modicum of agreement for partial pair correlation functions. The description of the short-range order, particularly when decomposed into contributions from Al and Cu centers, was too the most accurate among the three potentials. The main deficiency in the description of the local ordering lay in its inability to quantitatively capture the fractions of atoms with icosahedral and icosahedron-like ordering, which is not surprising given the absence of angular terms in the model. Densities were overestimated slightly, but less so than by the remaining potentials. Densities at melting temperature were in very good agreement (errors below 6%) with reference values for all compositions studied.

The apparent low transferability of EAM-ADP and of MEAM to liquid systems deserves further attention, perhaps warranting a study of the specific reasons underlying the deficiencies, with a view to improving parameterizations, or, if necessary, functional forms themselves, aiming to extend the range of applicability of empirical potentials to larger subsets of the Al-Cu phase diagram. A study like that falls outside the scope of this work, which instead focuses on highlighting the problem areas. For EAM-ADP problems become evident in Cu-rich systems, in particular for low temperatures. For MEAM the description is impaired for Al-rich systems, in the entire liquid temperature range, but to a lesser extent. Neither of these potentials offers a qualitatively correct picture of the liquid state of Al-Cu across all compositions and temperatures. In defense of EAM-ADP and MEAM, we point out that these potentials have been designed with focus on solid phases (and specific solid phases in the case of EAM-ADP), as evidenced by the choice of quantities used during parameterization. In this context, and with poor transferability of empirical potentials being widely recognized, the observed failings are perhaps less surprising. The main result of this work is confirming the non-transferability and examining how it manifests, with particular attention paid to local ordering.

In the view of the above, we finish with two broad conclusions. First, for studies of *liquid* Al-Cu at the empirical potential level we firmly deem the Gupta potential to constitute the model of choice, with more complex models offered by EAM-ADP and MEAM yielding predictions in poorer agreement with DFT and experimental results. Second, despite recent efforts and advances, a coherent and transferable description of the Al-Cu system remains elusive, and there is still a need for novel and thoroughly validated classical models.

Acknowledgments

We acknowledge the support of the Polish Ministry of Science and Higher Education (grant IP2012 043972) and of the TASK Academic Computer Centre (Gdańsk, Poland). This research was also supported in part by the PL-Grid Infrastructure (grant POIG.02.03.00-00-096/10). We extend our gratitude to Prof. Songyou Wang for providing us with the raw reference data and to Profs. Stepan Mudry and Ihor

Shtablavyi from the Department of Metal Physics, Ivan Franko University of Lviv, Ukraine for fruitful discussions and comments on the manuscript.

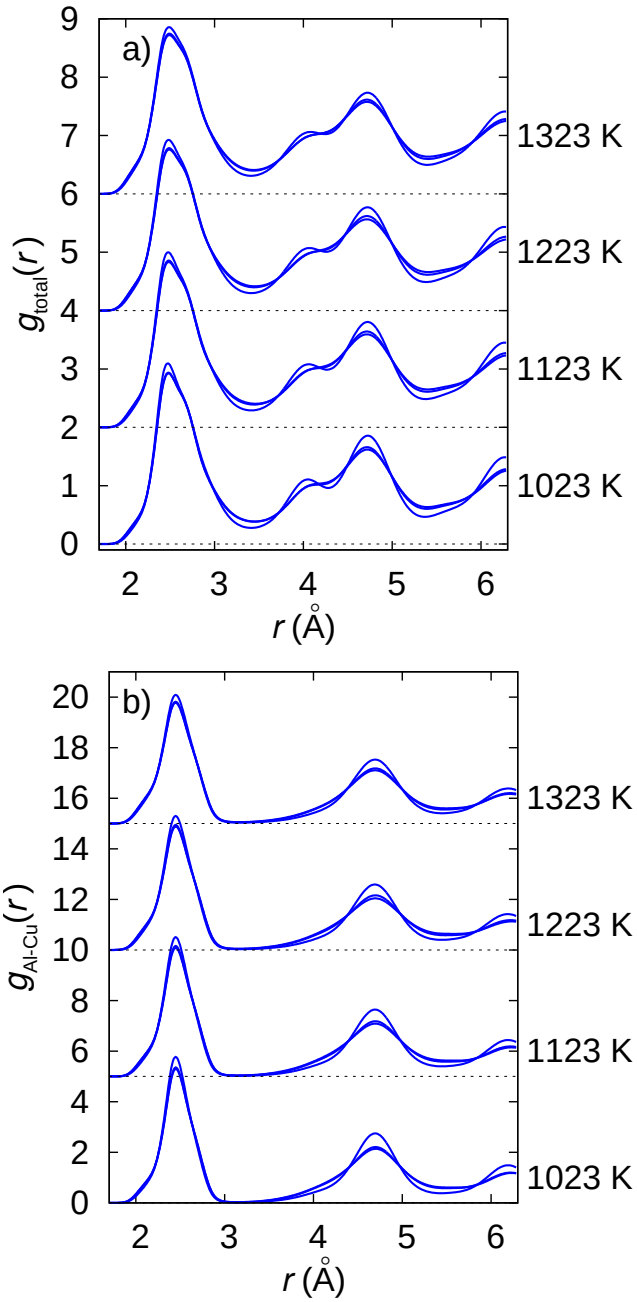

Figure 2: Total (panel a) and Al-Cu (panel b) pair correlation functions of the $Al_{60}Cu_{40}$ alloy obtained with EAM-ADP for four temperatures for three different initial conditions. Values for 1123 K, 1223 K and 1323 K were shifted by an integer number of units, this is indicated with dashed horizontal lines.

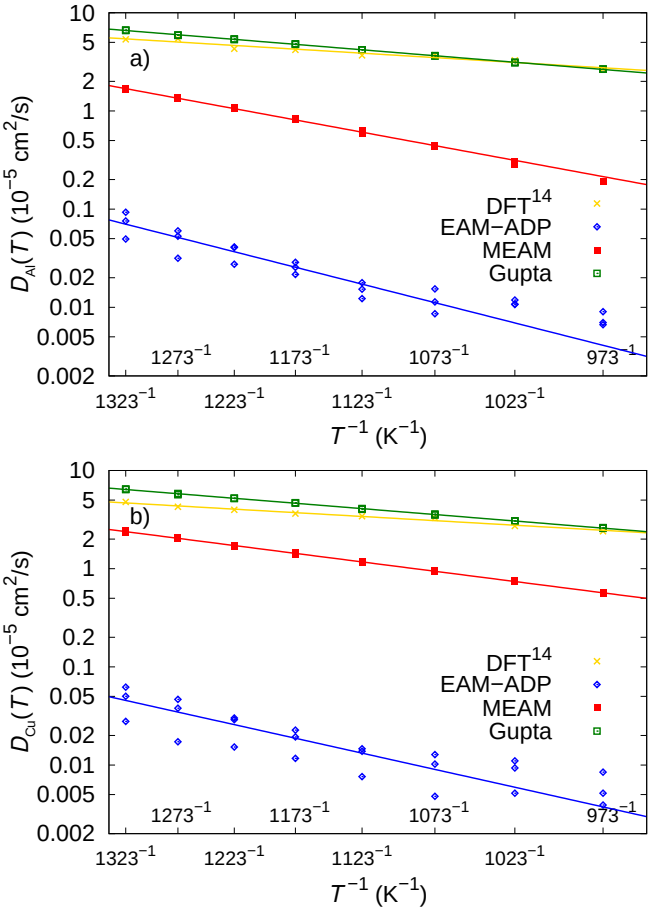

Figure 3: Self-diffusion coefficient of Al (panel a) and Cu (panel b) in liquid $Al_{60}Cu_{40}$ alloy as a function of temperature (points). Lines are results of Arrhenius fits to the datapoints.

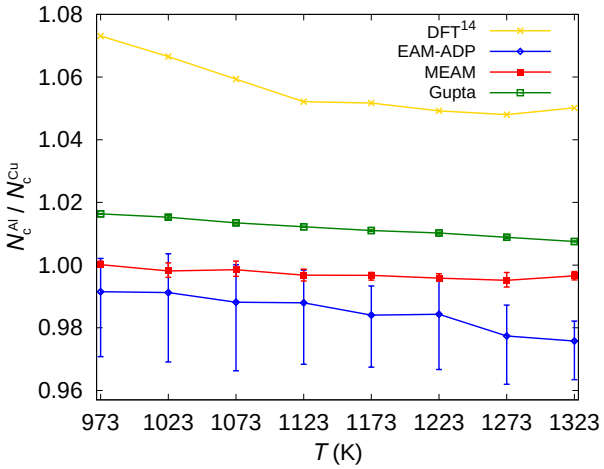

Figure 4: Coordination number ratio (Al to Cu) of liquid $Al_{60}Cu_{40}$ for eight temperatures. Points represent averages over three calculations with differing initial conditions, error bars denote minimum and maximum values obtained from the three calculations.

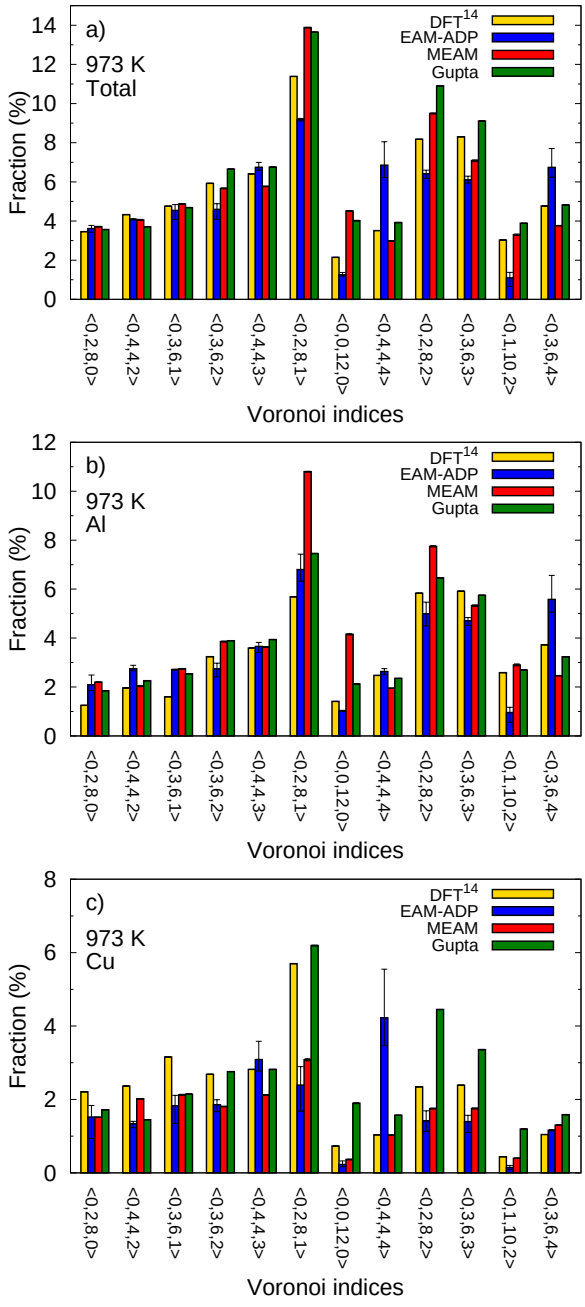

Figure 5: Frequency distributions of the most abundant structures in liquid $Al_{60}Cu_{40}$ at 973 K – averaged over atomic species (panel a), with Al as centers (panel b), with Cu as centers (panel c). The bars represent averages over three calculations with differing initial conditions, error bars denote minimum and maximum values obtained from the three calculations. Heights of the bars in panels b and c add up to the heights shown in panel a.

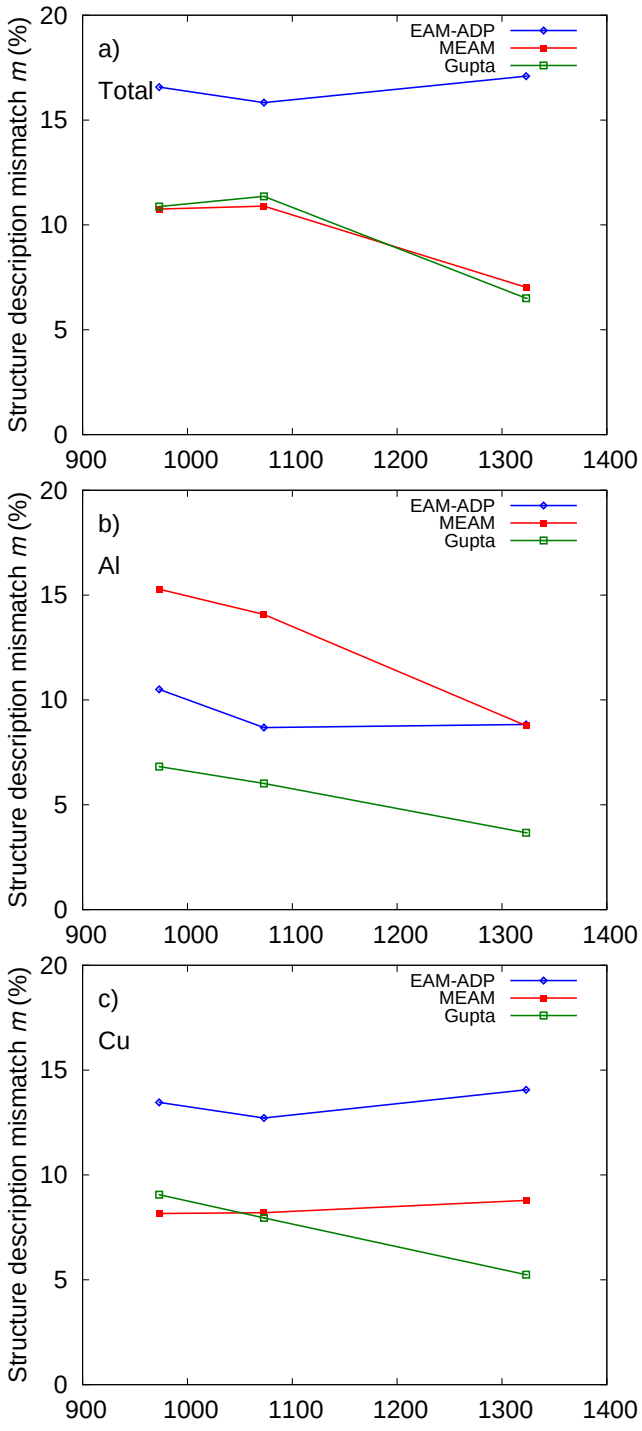

Figure 6: Structure description mismatch between the predictions of the three studied potentials and DFTMD results (Ref. [34]), calculated as a weighted relative error (cf. (21)) in the fractions of the most abundant structures in liquid $Al_{60}Cu_{40}$ – averaged over atomic species (panel a), with Al as centers (panel b), with Cu as centers (panel c).

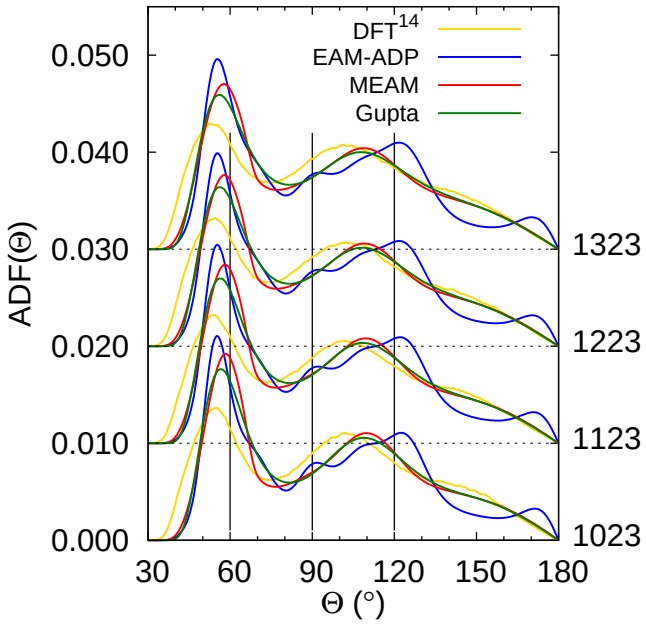

Figure 7: Angular distribution function of liquid $Al_{60}Cu_{40}$ for four temperatures. Values for 1123 K, 1223 K and 1323 K were shifted for clarity, this is indicated with dashed horizontal lines.

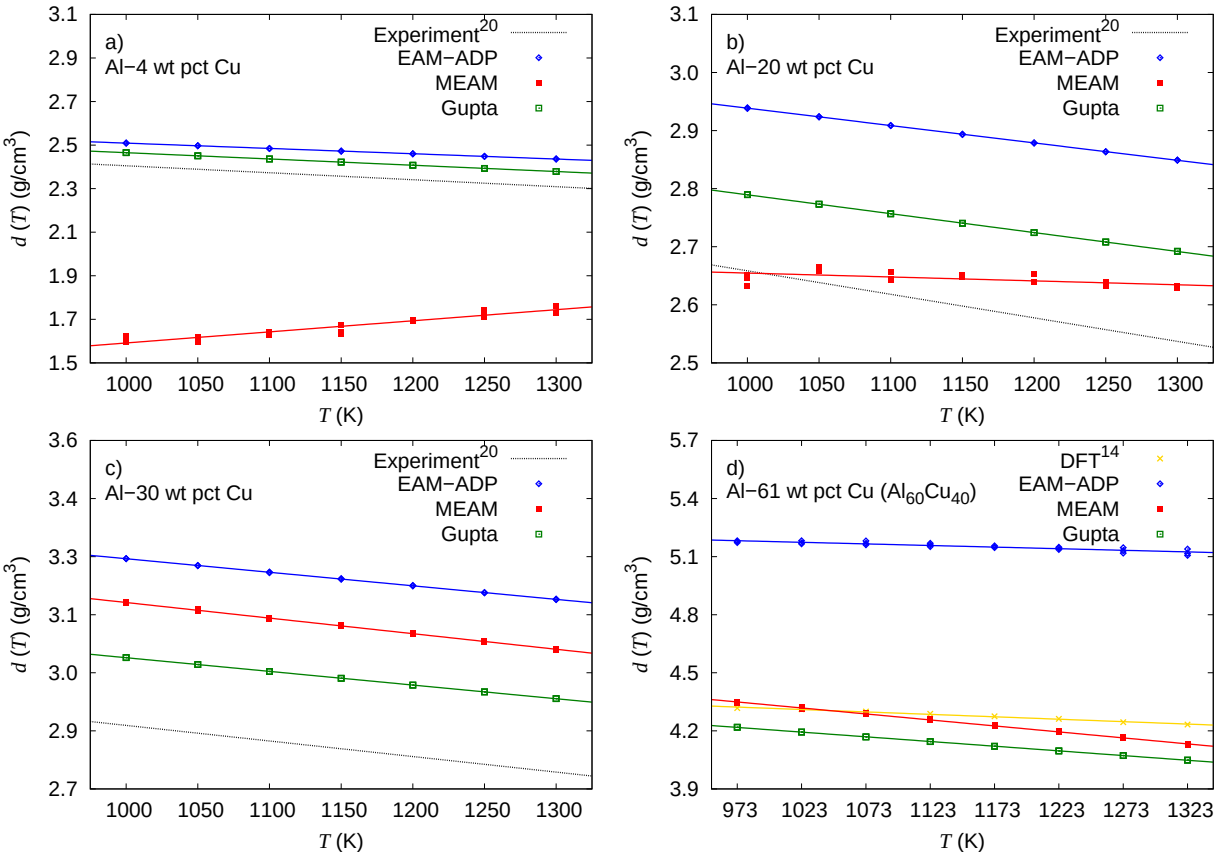

Figure 8: Temperature dependence of the density of Al-Cu alloys: Al-4 wt pct Cu (panel a), Al-20 wt pct Cu (panel b), Al-30 wt pct Cu (panel c), and Al-61 wt pct Cu ($Al_{60}Cu_{40}$, panel d). Points correspond to results of MD simulations, the lines are results of linear fits. The dotted black line denotes experimental results of Plevachuk *et al.* [42]. Crosses in panel d denote densities obtained from DFTMD by Wang *et al.* [34].

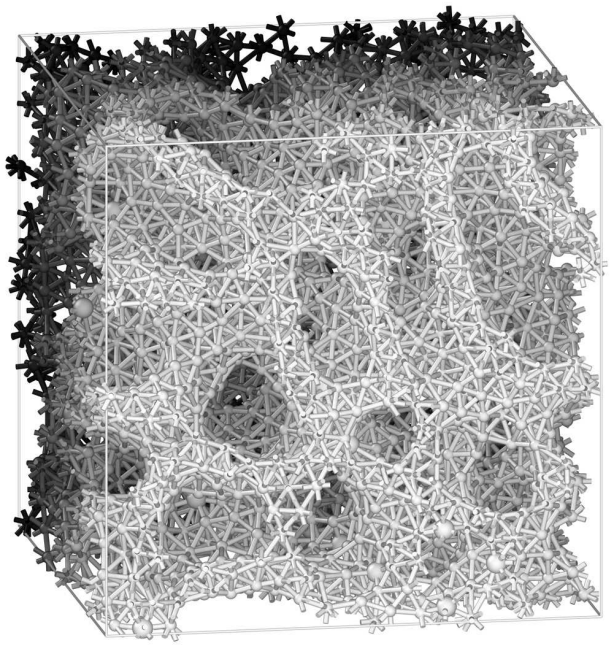

Figure 9: Example of an unphysical, foam-like structure predicted by the MEAM potential for Al-Cu alloys with low Cu content. Bonds are drawn between atoms closer than 3.6 Å (position of the first $g(r)$ minimum). Cu atoms are shown as larger spheres, Al atoms – as smaller spheres. Atoms and bonds are shaded according to their y coordinate as a visual cue. The illustration was generated using OVITO [77].

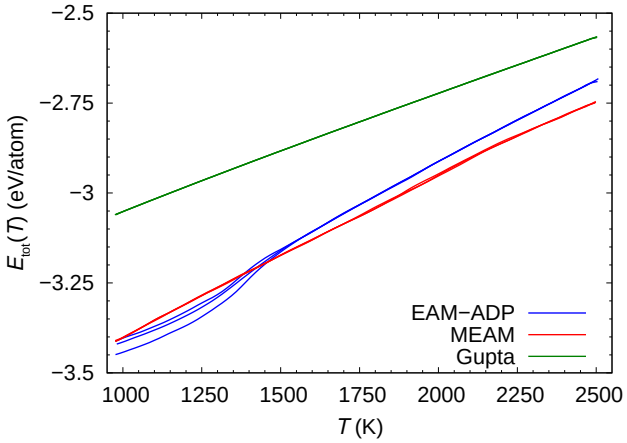

Figure 10: Total energy of the $Al_{60}Cu_{40}$ system during cooling, averaged over 2.5 ps windows. For EAM-ADP the change in slope between 1500 K and 1250 K is evidence of re-solidification, and the forking of the curves is due to the system being trapped in a different local energy minimum in each of the runs. Both problems are absent in simulations with the Gupta or MEAM potentials.

[1] F. Apostol, Y. Mishin, Interatomic potential for the Al-Cu system, Phys. Rev. B 83 (2011) 054116. doi:10.1103/PhysRevB.83.054116.
[2] B. Y. Thakore, S. G. Khambholja, P. H. Suthar, N. K. Bhatt, A. R. Jani, Collective modes and elastic constants of liquid Al83Cu17 binary alloy, Chinese Physics Letters 27 (9) (2010) 096203.
[3] A. Ancona, T. Sibillano, L. Tricarico, R. Spina, P. M. Lugarà, G. Basile, S. Schiavone, Comparison of two different nozzles for laser beam welding of {AA5083} aluminium alloy, Journal of Materials Processing Technology 164-165 (2005) 971 – 977. doi:http://dx.doi.org/10.1016/j.jmatprotec.2005.02.048.
[4] S. Mudry, I. Shtablavyi, J. Rybicki, Correlation between the structure in the liquid state and the structure in the solid state in the Al-Al2Cu eutectic alloy, Journal of Physical Studies 15 (1) (2011) 1601–1605.
[5] M. A. Talamantes-Silva, A. Rodríguez, J. Talamantes-Silva, S. Valtierra, R. Colás, Characterization of an Al-Cu cast alloy, Materials Characterization 59 (10) (2008) 1434 – 1439. doi:http://dx.doi.org/10.1016/j.matchar.2008.01.005.
[6] J. E. Spinelli, D. M. Rosa, I. L. Ferreira, A. Garcia, Influence of melt convection on dendritic spacings of downward unsteady-state directionally solidified Al-Cu alloys, Materials Science and Engineering: A 383 (2) (2004) 271 – 282. doi:http://dx.doi.org/10.1016/j.msea.2004.06.021.
[7] A. V. Yanilkin, V. S. Krasnikov, A. Y. Kuksin, A. E. Mayer, Dynamics and kinetics of dislocations in Al and Al-Cu alloy under dynamic loading, International Journal of Plasticity 55 (2014) 94 – 107. doi:http://dx.doi.org/10.1016/j.ijplas.2013.09.008.
[8] M. A. Zikry, Microstructurally engineered armor system for enhanced survivability through optimum energy and momentum dissipation, Tech. rep., North Carolina State University, Raleigh, NC 27695-7514 (6 2012).
[9] W. M. Lee, M. A. Zikry, Microstructural characterization of a high-strength aluminum alloy subjected to high strain-rate impact, Metallurgical and Materials Transactions A 42 (5) (2011) 1215–1221. doi:10.1007/s11661-010-0476-z.
[10] Y. J. Lv, M. Chen, Thermophysical properties of undercooled alloys: An overview of the molecular simulation approaches, Int. J. Mol. Sci. 12 (2011) 278 – 316. doi:http://dx.doi.org/10.3390/ijms12010278.
[11] B. Shen, C. Y. Liu, Y. Jia, G. Q. Yue, F. S. Ke, H. B. Zhao, L. Y. Chen, S. Y. Wang, C. Z. Wang, K. M. Ho, Molecular dynamics simulation studies of structural and dynamical properties of rapidly quenched Al, Journal of Non-Crystalline Solids 383 (2014) 13 – 20. doi:http://dx.doi.org/10.1016/j.jnoncrysol.2013.05.004.
[12] E. B. Tadmor, R. E. Miller, Modeling Materials: Continuum, Atomistic and Multiscale Techniques, Cambridge University Press, 2011.
[13] R. Gupta, Lattice relaxation at a metal surface, Phys. Rev. B 23 (1981) 6265–6270. doi:10.1103/PhysRevB.23.6265.
[14] M. Finnis, J. Sinclair, A simple empirical N-body potential for transition metals, Philosophical Magazine A 50 (1) (1984) 45–55.
[15] A. P. Sutton, J. Chen, Long-range Finnis-Sinclair potentials, Philosophical Magazine Letters 61 (3) (1990) 139–146. doi:10.1080/09500839008206493.
[16] H. Rafii-Tabar, A. P. Sutton, Long-range Finnis-Sinclair potentials for f.c.c. metallic alloys, Philosophical Magazine Letters 63 (4) (1991) 217–224. doi:10.1080/09500839108205994.
[17] T. Çagin, Y. Qi, H. Li, Y. Kimura, H. Ikeda, W. L. Johnson, W. A. Goddard III, The quantum Sutton-Chen many-body potential for properties of fcc metals, MRS Symposium Ser. 43.
[18] K. W. Jacobsen, J. K. Norskov, M. J. Puska, Interatomic interactions in the effective-medium theory, Phys. Rev. B 35 (1987) 7423–7442. doi:10.1103/PhysRevB.35.7423.
[19] K. W. Jacobsen, Bonding in metallic systems: An effective medium approach, Comments Condens. Matter Phys. 14 (1988) 129–161.
[20] F. Ercolessi, E. Tosatti, M. Parrinello, Au (100) surface reconstruction, Phys. Rev. Lett. 57 (1986) 719–722. doi:10.1103/PhysRevLett.57.719.
[21] M. S. Daw, M. I. Baskes, Semiempirical, quantum mechanical calculation of hydrogen embrittlement in metals, Phys. Rev. Lett. 50 (1983) 1285–1288. doi:10.1103/PhysRevLett.50.1285.
[22] M. S. Daw, M. I. Baskes, Embedded-atom method: Derivation and application to impurities, surfaces, and other defects in metals, Phys. Rev. B 29 (1984) 6443–6453. doi:10.1103/PhysRevB.29.6443.
[23] M. S. Daw, Model of metallic cohesion: The embedded-atom method, Phys. Rev. B 39 (1989) 7441–7452. doi:10.1103/PhysRevB.39.7441.
[24] N. Zonias, Atomistic simulations of semiconductor and metallic nanoparticles, Ph.D. thesis, University of Southampton, Southampton (7 2011).
[25] G. P. Purja Pun, Y. Mishin, Development of an interatomic potential for the Ni-Al system, Philosophical Magazine 89 (2009) 3245–3267. doi:10.1080/14786430903258184.
[26] I. G. Brodova, P. S. Popel', N. M. Barbin, N. A. Vatolin, *Iskhodnye rasplavy kak osnova formirovaniya struktury i svoistv alyuminievykh splavov* (Initial Melts as the Basis for Forming the Structure and Properties of Aluminum Alloys), UrO RAN (Ural Div., Russ. Acad. Sci.), Ekaterinburg, 2005.
[27] H. E. A. Huitema, J. P. van der Eerden, J. J. M. Janssen, H. Human, Thermodynamics and kinetics of homogeneous crystal nucleation studied by computer simulation, Phys. Rev. B 62 (2000) 14690–14702. doi:10.1103/PhysRevB.62.14690.
[28] B.-J. Lee, W.-S. Ko, H.-K. Kim, E.-H. Kim, The modified embedded-atom method interatomic potentials and recent progress in atomistic simulations, Calphad 34 (4) (2010) 510 – 522. doi:http://dx.doi.org/10.1016/j.calphad.2010.10.007.
[29] J. R. Morris, U. Dahlborg, M. Calvo-Dahlborg, Recent developments and outstanding challenges in theory and modeling of liquid metals, Journal of Non-Crystalline Solids 353 (32-40) (2007) 3444 – 3453. doi:http://dx.doi.org/10.1016/j.jnoncrysol.2007.05.159.
[30] C. V. Singh, D. H. Warner, An atomistic-based hierarchical multiscale examination of age hardening in an Al-Cu alloy, Metallurgical and Materials Transactions A 44 (6) (2013) 2625–2644. doi:10.1007/s11661-013-1614-1.

[31] C. Kuiying, L. Hongbo, L. Xiaoping, H. Qiyong, H. Zhuangqi, Molecular dynamics simulation of local structure of aluminium and copper in supercooled liquid and solid state by using EAM, Journal of Physics: Condensed Matter 7 (12) (1995) 2379.
[32] Y. Qi, T. Çağin, Y. Kimura, W. A. Goddard III, Viscosities of liquid metal alloys from nonequilibrium molecular dynamics, Journal of computer-aided materials design 8 (2-3) (2001) 233–243.
[33] X. J. Han, M. Chen, Z. Y. Guo, Thermophysical properties of undercooled liquid Au-Cu alloys from molecular dynamics simulations, Journal of Physics: Condensed Matter 16 (6) (2004) 705.
[34] S. Y. Wang, M. J. Kramer, M. Xu, S. Wu, S. G. Hao, D. J. Sordelet, K. M. Ho, C. Z. Wang, Experimental and *ab initio* molecular dynamics simulation studies of liquid Al60Cu40 alloy, Phys. Rev. B 79 (2009) 144205. doi:10.1103/PhysRevB.79.144205.
[35] B. Jelinek, S. Groh, M. F. Horstemeyer, J. Houze, S. G. Kim, G. J. Wagner, A. Moitra, M. I. Baskes, Modified embedded atom method potential for Al, Si, Mg, Cu, and Fe alloys, Phys. Rev. B 85 (2012) 245102. doi:10.1103/PhysRevB.85.245102.
[36] J. Dziedzic, E. Principi, J. Rybicki, Analysis of the mixing rules for the Stillinger-Weber potential: a case-study of Ge-Si interactions in the liquid phase, Journal of Non-Crystalline Solids 352 (40-41) (2006) 4232 – 4241. doi:http://dx.doi.org/10.1016/j.jnoncrysol.2006.07.017.
[37] B. Sadigh, P. Erhart, A. Stukowski, A. Caro, Composition-dependent interatomic potentials: A systematic approach to modelling multicomponent alloys, Philosophical Magazine 89 (34-36) (2009) 3371–3391. doi:10.1080/14786430903292373.
[38] J. Cai, Y. Y. Ye, Simple analytical embedded-atom-potential model including a long-range force for fcc metals and their alloys, Phys. Rev. B 54 (1996) 8398–8410. doi:10.1103/PhysRevB.54.8398.
[39] X.-Y. Liu, C.-L. Liu, L. J. Borucki, A new investigation of copper's role in enhancing Al-Cu interconnect electromigration resistance from an atomistic view, Acta Materialia 47 (11) (1999) 3227 – 3231. doi:http://dx.doi.org/10.1016/S1359-6454(99)00186-X.
[40] B.-J. Lee, J.-H. Shim, M. I. Baskes, Semiempirical atomic potentials for the fcc metals Cu, Ag, Au, Ni, Pd, Pt, Al, and Pb based on first and second nearest-neighbor modified embedded atom method, Phys. Rev. B 68 (2003) 144112. doi:10.1103/PhysRevB.68.144112.
[41] J. Brillo, S. M. Chathoth, M. M. Koza, A. Meyer, Liquid Al80Cu20: Atomic diffusion and viscosity, Applied Physics Letters 93 (12). doi:http://dx.doi.org/10.1063/1.2977863.
[42] Y. Plevachuk, V. Sklyarchuk, A. Yakymovych, S. Eckert, B. Willers, K. Eigenfeld, Density, viscosity, and electrical conductivity of hypoeutectic Al-Cu liquid alloys, Metallurgical and Materials Transactions A 39 (12) (2008) 3040–3045. doi:10.1007/s11661-008-9659-2.
[43] U. Dahlborg, M. Besser, M. Calvo-Dahlborg, S. Janssen, F. Juranyi, M. J. Kramer, J. R. Morris, D. J. Sordelet, Diffusion of Cu in AlCu alloys of different composition by quasielastic neutron scattering, Journal of Non-Crystalline Solids 353 (32-40) (2007) 3295 – 3299. doi:http://dx.doi.org/10.1016/j.jnoncrysol.2007.05.074.
[44] U. Dahlborg, M. Besser, M. J. Kramer, J. R. Morris, M. Calvo-Dahlborg, Atomic dynamics in molten AlCu alloys of different compositions and at different temperatures by cold neutron scattering, Physica B: Condensed Matter 412 (2013) 50 – 60. doi:http://dx.doi.org/10.1016/j.physb.2012.12.019.
[45] J.-H. Lee, S. Liu, H. Miyahara, R. Trivedi, Diffusion-coefficient measurements in liquid metallic alloys, Metallurgical and Materials Transactions B 35 (5) (2004) 909–917. doi:10.1007/s11663-004-0085-6.
[46] B. Zhang, A. Griesche, A. Meyer, Diffusion in Al-Cu melts studied by time-resolved X-ray radiography, Phys. Rev. Lett. 104 (2010) 035902. doi:10.1103/PhysRevLett.104.035902.
[47] J. Brillo, I. Egry, J. Westphal, Density and thermal expansion of liquid binary Al-Ag and Al-Cu alloys, International Journal of Materials Research 99 (2008) 162–167. doi:10.3139/146.101623.
[48] J. Friedel, The Physics of Metals, Vol. 1, Pergamon, London, 1969, edited by J. M. Ziman.
[49] J. Fu, J. Zhao, Gupta potential for rare earth elements of the fcc phase: lanthanum and cerium, Modelling and Simulation in Materials Science and Engineering 21 (6) (2013) 065003.
[50] Ducastelle, F., Modules elastiques des metaux de transition, J. Phys. France 31 (11-12) (1970) 1055–1062. doi:10.1051/jphys:019700031011-120105500.
[51] V. Rosato, M. Guillope, B. Legrand, Thermodynamical and structural properties of f.c.c. transition metals using a simple tight-binding model, Philosophical Magazine A 59 (2) (1989) 321–336. doi:10.1080/01418618908205062.
[52] D. Kumar, V. Verma, K. Dharamvir, H. S. Bhatti, Theoretical study of silver nanostructures using Gupta potential, International Journal of Physics and Research 3 (2013) 33–44.
[53] F. Cleri, V. Rosato, Tight-binding potentials for transition metals and alloys, Phys. Rev. B 48 (1993) 22–33. doi:10.1103/PhysRevB.48.22.
URL `http://link.aps.org/doi/10.1103/PhysRevB.48.22`
[54] J. P. K. Doye, Lead clusters: Different potentials, different structures, Computational Materials Science 35 (3) (2006) 227 – 231, proceedings of the 4th International Conference on the Theory of Atomic and Molecular Clusters (TAMC-IV) The 4th International Conference on the Theory of Atomic and Molecular Clusters. doi:http://dx.doi.org/10.1016/j.commatsci.2004.07.009.
[55] J. P. K. Doye, Identifying structural patterns in disordered metal clusters, Phys. Rev. B 68 (2003) 195418. doi:10.1103/PhysRevB.68.195418.
[56] E. G. Noya, J. P. K. Doye, D. J. Wales, A. Aguado, Geometric magic numbers of sodium clusters: Interpretation of the melting behaviour, The European Physical Journal D 43 (1-3) (2007) 57–60. doi:10.1140/epjd/e2007-00092-x.
[57] C. Rey, L. J. Gallego, J. García-Rodeja, J. A. Alonso, M. P. Iñiguez, Molecular-dynamics study of the binding energy and melting of transition-metal clusters, Phys. Rev. B 48 (1993) 8253–8262. doi:10.1103/PhysRevB.48.8253.
[58] N. Y. Sdobnyakov, P. V. Komarov, D. N. Sokolov, V. M. Samsonov, Study of the thermodynamic characteristics of

gold nanoclusters using a Gupta many-body potential, The Physics of Metals and Metallography 111 (1) (2011) 13–20. doi:10.1134/S0031918X11010121.
[59] V. Bocchetti, H. T. Diep, Monte Carlo simulation of melting and lattice relaxation of the (111) surface of silver, Surface Science 614 (2013) 46 – 52. doi:http://dx.doi.org/10.1016/j.susc.2013.04.003.
[60] A. Posada-Amarillas, I. L. Garzón, Microstructural analysis of simulated liquid and amorphous Ni, Phys. Rev. B 53 (1996) 8363–8368. doi:10.1103/PhysRevB.53.8363.
[61] F. Willaime, C. Massobrio, Development of an N-body interatomic potential for hcp and bcc zirconium, Phys. Rev. B 43 (1991) 11653–11665. doi:10.1103/PhysRevB.43.11653.
[62] Y. Mishin, D. Farkas, M. J. Mehl, D. A. Papaconstantopoulos, Interatomic potentials for monoatomic metals from experimental data and *ab initio* calculations, Phys. Rev. B 59 (1999) 3393–3407. doi:10.1103/PhysRevB.59.3393.
URL `http://link.aps.org/doi/10.1103/PhysRevB.59.3393`
[63] Y. Mishin, M. J. Mehl, D. A. Papaconstantopoulos, A. F. Voter, J. D. Kress, Structural stability and lattice defects in copper: *Ab initio*, tight-binding, and embedded-atom calculations, Phys. Rev. B 63 (2001) 224106. doi:10.1103/PhysRevB.63.224106.
URL `http://link.aps.org/doi/10.1103/PhysRevB.63.224106`
[64] C. Li, D. Li, X. Tao, H. Chen, Y. Ouyang, Molecular dynamics simulation of diffusion bonding of Al-Cu interface, Modelling and Simulation in Materials Science and Engineering 22 (6) (2014) 065013.
[65] M. I. Baskes, Modified embedded-atom potentials for cubic materials and impurities, Phys. Rev. B 46 (1992) 2727–2742. doi:10.1103/PhysRevB.46.2727.
URL `http://link.aps.org/doi/10.1103/PhysRevB.46.2727`
[66] M. I. Baskes, R. A. Johnson, Modified embedded atom potentials for hcp metals, Modelling and Simulation in Materials Science and Engineering 2 (1) (1994) 147.
URL `http://stacks.iop.org/0965-0393/2/i=1/a=011`
[67] B.-J. Lee, M. I. Baskes, Second nearest-neighbor modified embedded-atom-method potential, Phys. Rev. B 62 (2000) 8564–8567. doi:10.1103/PhysRevB.62.8564.
URL `http://link.aps.org/doi/10.1103/PhysRevB.62.8564`
[68] B.-J. Lee, M. I. Baskes, H. Kim, Y. K. Cho, Second nearest-neighbor modified embedded atom method potentials for bcc transition metals, Phys. Rev. B 64 (2001) 184102. doi:10.1103/PhysRevB.64.184102.
URL `http://link.aps.org/doi/10.1103/PhysRevB.64.184102`
[69] Y.-M. Kim, B.-J. Lee, M. I. Baskes, Modified embedded-atom method interatomic potentials for Ti and Zr, Phys. Rev. B 74 (2006) 014101. doi:10.1103/PhysRevB.74.014101.
[70] S. Nosé, A unified formulation of the constant temperature molecular dynamics methods, The Journal of Chemical Physics 81 (1) (1984) 511–519. doi:http://dx.doi.org/10.1063/1.447334.
[71] W. G. Hoover, Canonical dynamics: Equilibrium phase-space distributions, Phys. Rev. A 31 (1985) 1695–1697. doi:10.1103/PhysRevA.31.1695.
[72] A. C. Brańka, M. Kowalik, K. W. Wojciechowski, Generalization of the Nosé-Hoover approach, The Journal of Chemical Physics 119 (2003) 1929–1936. doi:10.1063/1.1584427.
[73] W. Shinoda, M. Shiga, M. Mikami, Rapid estimation of elastic constants by molecular dynamics simulation under constant stress, Phys. Rev. B 69 (2004) 134103. doi:10.1103/PhysRevB.69.134103.
[74] S. Plimpton, Fast parallel algorithms for short-range molecular dynamics, Journal of Computational Physics 117 (1) (1995) 1 – 19. doi:http://dx.doi.org/10.1006/jcph.1995.1039.
[75] W. M. Haynes (Ed.), Handbook of Chemistry and Physics, 95th Edition, CRC Press, 2014-2015.
[76] C. H. Rycroft, VORO++: A three-dimensional Voronoi cell library in C++, Chaos 19 (4). doi:http://dx.doi.org/10.1063/1.3215722.
[77] A. Stukowski, Visualization and analysis of atomistic simulation data with OVITO - the open visualization tool, Modelling and Simulation in Materials Science and Engineering 18 (1) (2010) 015012.